ELSEVIER

Journal of Organometallic Chemistry 650 (2002) 133–140

Journal of Organometallic Chemistry

www.elsevier.com/locate/jorganchem

Mixed-metal cluster chemistry
Part 20. Syntheses, crystal structures and electrochemical studies of $W_2Ir_2(\mu\text{-}L)(CO)_8(\eta^5\text{-}C_5H_4Me)_2$ (L = dppe, dppf)☆

Jonathan P. Blitz [1], Nigel T. Lucas, Mark G. Humphrey *

Department of Chemistry, Australian National University, Canberra, ACT 0200, Australia

Received 11 November 2001; accepted 15 January 2002

Abstract

The 60-electron tetrahedral clusters $W_2Ir_2(\mu\text{-}L)(CO)_8(\eta^5\text{-}C_5H_4Me)_2$ [L = dppe (**2**), dppf (**3**)] have been prepared from reaction between $W_2Ir_2(CO)_{10}(\eta^5\text{-}C_5H_4Me)_2$ (**1**) and the corresponding diphosphine in 52 and 66% yields, respectively. A structural study of **2** reveals that three edges of a WIr_2 face are spanned by bridging carbonyls, that the iridium-ligated diphosphine coordinates diaxially and that the tungsten-bound methylcyclopentadienyls coordinate axially and apically with respect to the plane of bridging carbonyls. A structural study of **3** reveals that the dppf ligand bridges an Ir–Ir bond which is also spanned by a bridging carbonyl; tungsten-ligated methylcyclopentadienyl ligands and terminal carbonyls result in electronic asymmetry (17e and 19e iridium atoms) in the electron-precise cluster. Both clusters show two reversible one-electron oxidation processes and an irreversible two-electron reduction; the dppf-containing cluster **3** has a further, irreversible, one-electron oxidation process. UV–vis-NIR spectroelectrochemical studies of the $\mathbf{2} \rightarrow \mathbf{2}^+ \rightarrow \mathbf{2}^{2+}$ progression reveal the appearance of a low-energy transition on oxidation to $\mathbf{2}^+$ which persists on further oxidation to $\mathbf{2}^{2+}$. © 2002 Published by Elsevier Science B.V.

Keywords: Tungsten; Iridium; Carbonyl; Cyclopentadienyl; Cluster; Phosphine

1. Introduction

There has been significant recent interest in the phosphine substitution chemistry of mixed-metal clusters [2,3]. We have focussed on mixed Group 6–iridium clusters, with studies delineating isomer structures and carbonyl fluxionality pathways [1,4–13]. A fundamentally important concern in cluster chemistry is tuning cluster electronic environment by peripheral ligand modification. One attractive way to accomplish this is by replacement of strong electron-withdrawing carbonyl ligands by electron-donating phosphines. We recently reported exploring this possibility for the clusters $W_nIr_{4-n}(CO)_{12-n}(\eta^5\text{-}C_5H_4Me)_n$ ($n = 1$, 2) with the monodentate phosphine PMe_3, in a combined UV–vis-NIR and IR spectroelectrochemistry and density functional theory (DFT) study [1]. However, the bis-adducts were unstable, precluding a detailed study. We report herein the extension of this study to embrace the bidentate ligands dppe and dppf, crystallographic characterization of the products which reveals an unusual ligand disposition for the dppf adduct, and cyclic voltammetric studies which reveal *two* electrochemically reversible oxidation processes; the last-mentioned have been probed by UV–vis-NIR spectroelectrochemistry, revealing an unusual low-energy transition on the first oxidation which persists upon the second oxidation.

2. Results and discussion

2.1. Syntheses of $W_2Ir_2(\mu\text{-}L)(CO)_8(\eta^5\text{-}C_5H_4Me)_2$ [L = dppe (2), dppf (3)]

The reactions of $W_2Ir_2(CO)_{10}(\eta^5\text{-}C_5H_4Me)_2$ (**1**) with one equivalent of dppe or dppf proceed in dichloromethane at room temperature to afford the substitution products $W_2Ir_2(\mu\text{-dppe})(CO)_8(\eta^5\text{-}C_5H_4Me)_2$ (**2**) or

☆ Part 19: see Ref. [1].

* Corresponding author. Tel.: +61-2-6125-2927; fax: +61-2-6125-0760.

E-mail address: mark.humphrey@anu.edu.au (M.G. Humphrey).

[1] On leave from Eastern Illinois University, USA.

0022-328X/02/$ - see front matter © 2002 Published by Elsevier Science B.V.
PII: S0022-328X(02)01201-9

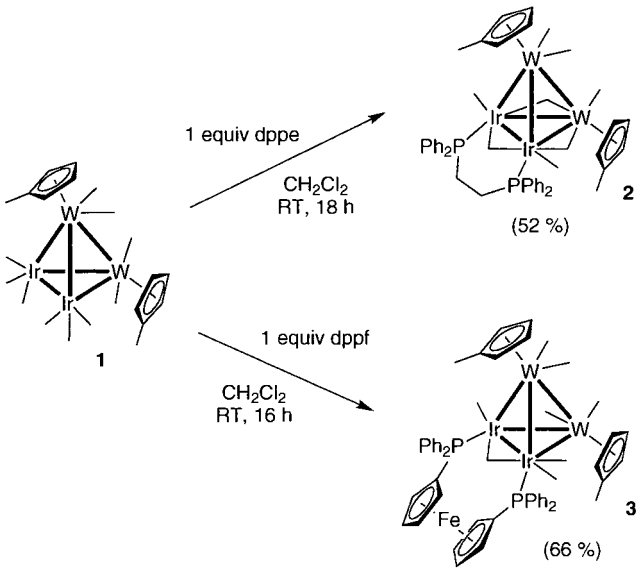

Scheme 1. Syntheses of $W_2Ir_2(\mu\text{-dppe})(CO)_8(\eta^5\text{-}C_5H_4Me)_2$ (**2**) and $W_2Ir_2(\mu\text{-dppf})(CO)_8(\eta^5\text{-}C_5H_4Me)_2$ (**3**).

$W_2Ir_2(\mu\text{-dppf})(CO)_8(\eta^5\text{-}C_5H_4Me)_2$ (**3**), respectively, as the major products (Scheme 1). Clusters **2** and **3** have been characterized by a combination of IR, ^{1}H- and ^{31}P-NMR spectroscopies, SI mass spectrometry, and satisfactory microanalyses. Infrared spectra suggest the presence of edge-bridging carbonyl ligands in both complexes, which contrasts with the all-terminal geometry of the precursor **1**. The ^{1}H-NMR spectra contain signals assigned to methylcyclopentadienyl, phenyl, methylene (**2**), and 1,1′-ferrocenyl (**3**) groups in the appropriate ratios. The ^{31}P-NMR spectra contain broad resonances suggestive of fluxional processes. We have previously reported variable temperature ^{31}P-NMR and ^{13}C-NMR spectra for the related $W_2Ir_2(\mu\text{-L})(CO)_8(\eta^5\text{-}C_5H_5)_2$ [L = dppm (**4**), dppe (**5**)], for which a fluxional process involving rotation at the apical $W(CO)_2(\eta^5\text{-}C_5H_5)$ unit was proposed [13]; it is possible that a similar process is operative with **2** and **3**. The mass spectra of the new complexes contain molecular ions and fragment ions corresponding to stepwise loss of carbonyls; isotope patterns are consistent with the presence of two iridium atoms and two tungsten atoms. Clusters **2** and **3** were subjected to single-crystal X-ray diffraction studies.

2.2. X-ray structural studies of *2* and *3*

Figs. 1 and 2 show ORTEP plots of **2** and **3**, respectively, indicating the molecular structures and the atomic labelling schemes. Tables 1 and 2 contain selected bond lengths and angles for **2** and **3**, respectively, while Table 3 summarizes important crystal data and structure refinement details for the structural studies. Clusters **2** and **3** are substitution derivatives of

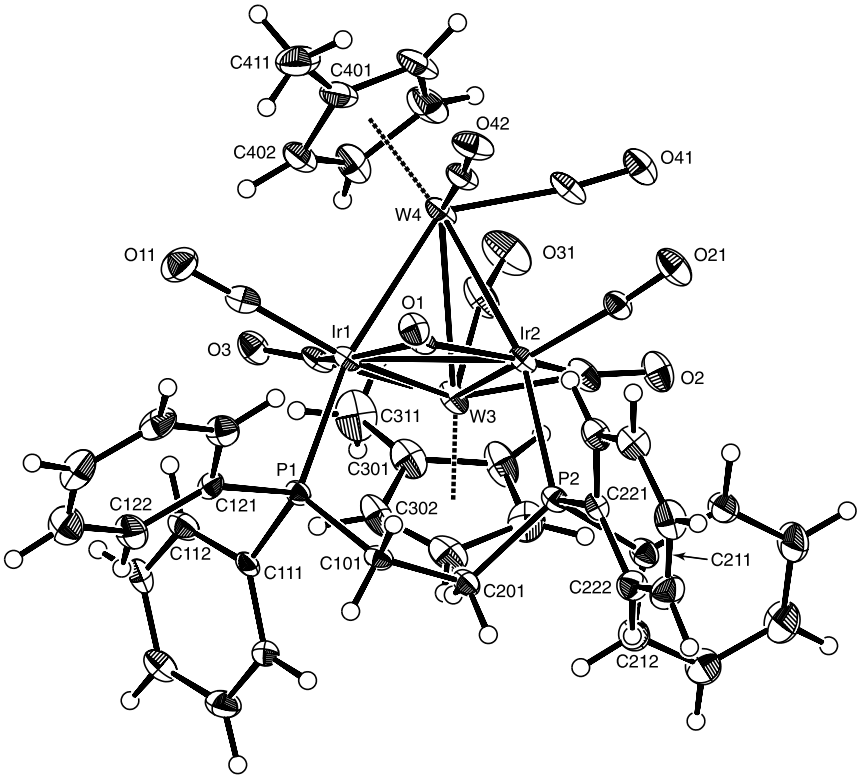

Fig. 1. ORTEP plot of $W_2Ir_2(\mu\text{-dppe})(\mu\text{-}CO)_3(CO)_5(\eta^5\text{-}C_5H_4Me)_2$ (**2**) showing the molecular structure and atomic labelling scheme. Displacement ellipsoids are shown at the 30% probability level for the non-hydrogen atoms.

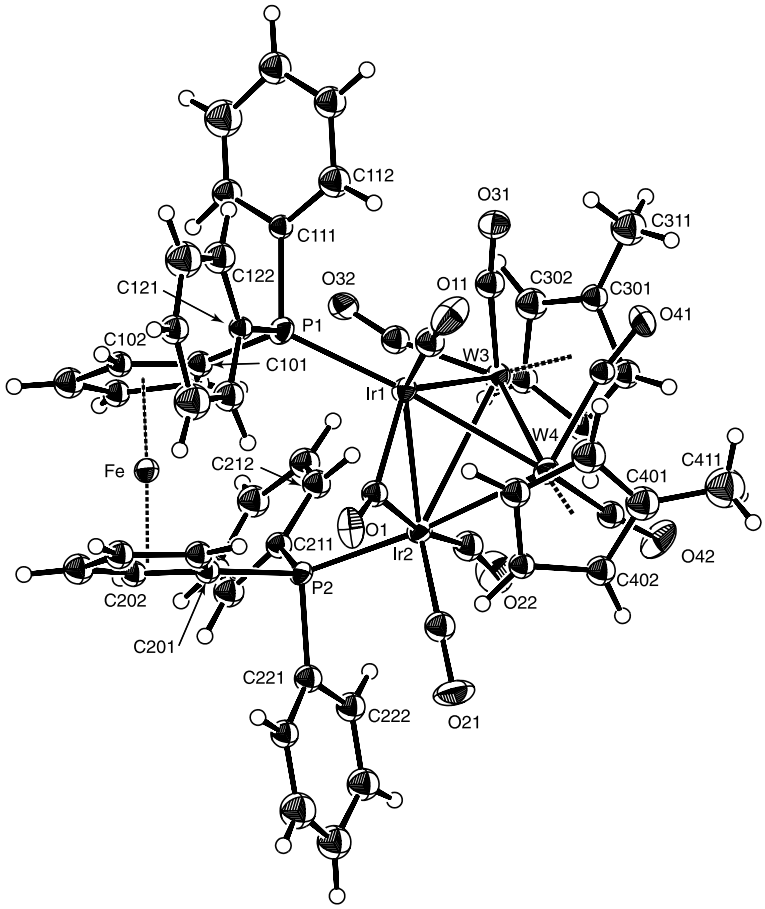

Fig. 2. ORTEP plot of $W_2Ir_2(\mu\text{-dppf})(\mu\text{-CO})(CO)_7(\eta^5\text{-}C_5H_4Me)_2$ (**3**) showing the molecular structure and atomic labelling scheme. Displacement ellipsoids are shown at the 30% probability level for the non-hydrogen atoms.

$W_2Ir_2(CO)_{10}(\eta\text{-}C_5H_4Me)_2$ (**1**) and have the W_2Ir_2 pseudotetrahedral framework of the precursor cluster and η^5-methylcyclopentadienyl groups coordinated to each tungsten. The bidentate phosphines dppe and dppf, respectively, span the two iridium atoms. The metal–metal bond lengths are, on average, longer than those of the precursor, with the exception being the Ir1–Ir2 bond in **2**, which is slightly shorter. The spread of Ir–W bond lengths within **3** is quite wide [Ir–W 2.742(1)–3.104(1) Å], which may be related to the non-18 valence electron count of the iridium atoms (see below) and the crowded coordination sphere of the cluster. The remaining coordination sites on **2** are occupied with three symmetrically-bridging carbonyl groups around the Ir1–Ir2–W3 face, two terminal Ir-bound carbonyls, and three W-bound carbonyls which adopt semi-bridging geometries, namely CO31 [$\angle$W3–C31–O31 163.2(9)°, W4···C31 2.779 Å, $\alpha = 0.44$], CO41 [$\angle$W4–C41–O41 173.5(8)°, Ir2···C41 3.114(8) Å, $\alpha = 0.58$] and CO42 [$\angle$W4–C42–O42 171.5(7)°, Ir2···C42 2.970(8)°, $\alpha = 0.50$] [Note: utilizing the Curtis-defined parameter $\alpha = (d_2 - d_1)/d_1$ for d_1 = short M–C distance, d_2 = long M···C distance, enables one to rapidly quantify the "semi-bridging" character of a carbonyl ligand. For semi-bridging carbonyls, $0.1 < \alpha < 0.6$ [14,15]]. The dppe ligand is diaxially-coordinated and the methylcyclopentadienyl groups axially- and apically-coordinated relative to the plane of bridging carbonyls; this configuration does not minimize steric interactions (radial, diaxial, apical coordination minimizes steric effects in tetrasubstituted clusters: see [11]), but it does agree with a configuration assignment of the cyclopentadienyl analogue $W_2Ir_2(\mu\text{-dppe})(CO)_8(\eta\text{-}C_5H_5)_2$ based on NMR studies [13]. The dppf-coordinated example **3** does not exhibit a distinct plane of bridging carbonyls, but rather one unsymmetrically bridging carbonyl group CO1 [Ir1–C 1.93(2), Ir2–C 2.12(2) Å] and three semi-bridging interactions CO31 [$\angle$W3–C31–O31 164(2)°, Ir1···2.57(2) Å, $\alpha = 0.29$], CO32 [$\angle$W3–C32–O32 165(2)°, Ir1···C32 2.89(2) Å, $\alpha = 0.48$] and CO41 [$\angle$W4–C41–O41 167(2)°, W3···2.89(2) Å, $\alpha = 0.47$]. The iridium-bound CO22 is also within bonding distance of W3 [3.07(2) Å] and the Ir2–C22–O22 bonds deviate significantly from linearity [165(2)°], but the α value (0.66) falls just outside the semi-bridging regime. If this weak interaction is considered as semi-bridging,

then CO22 and the bridging and semi-bridging carbonyls CO1 and CO31 define a pseudo-plane of bridging carbonyls, placing the dppf in axial sites and the methylcyclopentadienyls in radial and apical sites. Formal electron counting indicates that the cluster is electron precise for a tetrahedral geometry (60 CVE) but that the iridium centres within the cluster are not, with Ir1 having 17 e and Ir2 having 19 e. The unsymmetrical nature of the bridging ligand CO1 and semi-bridging interactions Ir1···CO31 and Ir1···CO32 presumably help to alleviate this electronic imbalance.

2.3. Electrochemical studies of **2** and **3**

Both clusters **2** and **3** are electron precise (60 CVE) in the resting state. Cyclic voltammetric scans of **2** and **3** using a switching potential of 1.7 V show two successive reversible/quasi-reversible cluster-centred oxidation processes followed, in the case of **3**, by an irreversible oxidation process (Table 4); this behaviour contrasts with that of the precursor **1**, for which the second oxidation process is irreversible, but is consistent with the mono-phosphine complex $W_2Ir_2(CO)_9(PMe_3)(\eta^5\text{-}C_5H_4Me)_2$ (**6**) [1], the electron-donating ligands stabilizing the dicationic state. Replacing dppe by dppf in proceeding from **2** to **3** results in one additional accessible oxidation process, which it is tempting to ascribe to oxidation at the ferrocenyl iron but the specific assignment of the three oxidation processes for **3** is unclear. A small increase in reversibility for the third oxidation processes in **3** was observed when the scan rate was increased. The electron-transfer stoichiometries for the two reversible oxidation processes in **2** and **3** have been quantified as one-electron processes using controlled potential coulometry. Clusters **2** and **3** exhibit irreversible reduction processes which are assigned as two-electron in nature by peak height comparison (Table 4). Increasing the scan rate and/or cooling the solution had no effect on the reversibility of these processes.

Examining the trends in oxidation and reduction potentials reveals that increasing phosphine incorporation (proceeding from **1** to **6** to **2**) results in increased ease of oxidation and increased difficulty in reduction, as would be expected if ligand replacement can be employed to systematically tune the cluster electronic environment. The reduction potential and the potential for the second oxidation for **3** are somewhat anomalous, presumably reflecting the incorporation of the redox-active iron centre.

Table 1
Selected bond lengths (Å) and angles (°) for $W_2Ir_2(\mu\text{-dppe})(\mu\text{-CO})_3(CO)_5(\eta^5\text{-}C_5H_4Me)_2$ (**2**)

Bond lengths			
Ir1–Ir2	2.6834(4)	W4–C42	1.852(8)
Ir1–W3	2.8907(4)	W3–Cp [a]	2.003
Ir1–W4	2.8446(4)	W4–Cp [a]	1.987
Ir2–W3	2.8844(4)	C1–O1	1.180(9)
Ir2–W4	2.9041(5)	C2–O2	1.168(9)
W3–W4	3.0951(5)	C3–O3	1.16(1)
Ir1–P1	2.305(2)	C11–O11	1.14(1)
Ir2–P2	2.295(2)	C21–O21	1.149(9)
Ir1–C1	2.062(8)	C31–O31	1.17(1)
Ir1–C2	2.124(8)	C41–O41	1.15(1)
Ir1–C3	2.087(7)	C42–O42	1.15(1)
Ir1–C11	2.169(7)		
Ir2–C21	2.116(9)	Ir2···C41	3.114(8)
W3–C31	2.155(9)	Ir2···C42	2.970(8)
W4–C41	1.883(9)	W4···C31	2.779(9)
Bond angles			
Ir2–Ir1–W3	62.19(1)	Ir1–C1–O1	140.5(6)
Ir2–Ir1–W4	63.30(1)	Ir2–C1–O1	138.9(7)
W3–Ir1–W4	65.31(1)	Ir2–C2–O2	132.3(7)
Ir1–Ir2–W3	62.43(1)	W3–C2–O2	143.1(7)
Ir1–Ir2–W4	61.06(1)	Ir1–C3–O3	134.4(6)
W3–Ir2–W4	64.65(1)	W3–C3–O3	140.6(6)
Ir1–W3–Ir2	55.37(1)	Ir1–C11–O11	179.2(7)
Ir1–W3–W4	56.62(1)	Ir2–C21–O21	176.3(8)
Ir2–W3–W4	57.98(1)	W3–C31–O31	163.2(9)
Ir1–W4–Ir2	55.64(1)	W4–C41–O41	173.5(8)
Ir1–W4–W3	58.06(1)	W4–C42–O42	171.5(7)
Ir2–W4–W3	57.37(1)		

[a] Indicates centroid of coordinated methylcyclopentadienyl ligand

Table 2
Selected bond lengths (Å) and angles (°) for $W_2Ir_2(\mu\text{-dppf})(\mu\text{-CO})(CO)_7(\eta^5\text{-}C_5H_4Me)_2$ (**3**)

Bond lengths			
Ir1–Ir2	2.798(1)	W3–Cp [a]	2.039
Ir1–W3	2.742(1)	W4–Cp [a]	2.015
Ir1–W4	2.834(1)	Fe–Cp1 [a]	1.651
Ir2–W3	3.104(1)	Fe–Cp2 [a]	1.647
Ir2–W4	2.881(1)	C1–O1	1.26(2)
W3–W4	3.037(1)	C11–O11	1.10(3)
Ir1–P1	2.357(6)	C21–O21	1.22(3)
Ir2–P2	2.386(6)	C22–O22	1.18(3)
Ir1–C1	1.93(2)	C31–O31	1.10(3)
Ir2–C1	2.12(2)	C32–O32	1.17(2)
Ir1–C11	1.86(3)	C41–O41	1.12(2)
Ir2–C21	1.85(2)	C42–O42	1.16(3)
Ir2–C22	1.85(3)		
W3–C31	2.00(3)	Ir1···C31	2.57(2)
W3–C32	1.95(2)	Ir1···C32	2.89(2)
W4–C41	1.97(2)	W3···C22	3.07(2)
W4–C42	1.96(2)	W3···C41	2.89(2)
Bond angles			
Ir2–Ir1–W3	68.16(3)	Ir1–C1–O1	138(2)
Ir2–Ir1–W4	61.54(3)	Ir2–C1–O1	134(2)
W3–Ir1–W4	65.98(3)	Ir1–C11–O11	175(2)
Ir1–Ir2–W3	55.07(3)	Ir2–C21–O21	172(2)
Ir1–Ir2–W4	59.86(3)	Ir2–C22–O22	165(2)
W3–Ir2–W4	60.85(3)	W3–C31–O31	164(2)
Ir1–W3–Ir2	56.77(3)	W3–C32–O32	165(2)
Ir1–W3–W4	58.47(3)	W4–C41–O41	167(2)
Ir2–W3–W4	55.94(3)	W4–C42–O42	169(2)
Ir1–W4–Ir2	58.60(3)		
Ir1–W4–W3	55.54(3)		
Ir2–W4–W3	63.21(3)		

[a] Indicates centroid of coordinated methylcyclopentadienyl ligand.

Table 3
Crystal data and structure refinement details for **2** and **3**

	2	**3**
Empirical formula	$C_{46}H_{38}Ir_2O_8P_2W_2 \cdot H_2O$	$C_{54}H_{42}FeIr_2O_8P_2W_2 \cdot CHCl_3$
Formula weight	1548.89	1808.23
Crystal system	Monoclinic	Triclinic
Space group	$C2/c$ (# 15)	$P\bar{1}$ (# 2)
a (Å)	26.2666(2)	12.2687(6)
b (Å)	18.2666(2)	13.4221(7)
c (Å)	21.0919(2)	17.513(1)
α (°)		79.334(3)
β (°)	119.3988(4)	71.952(3)
γ (°)		77.207(3)
V (Å^3)	8816.7(1)	2629.8(3)
D_{calc} (g cm^{-3})	2.33	2.28
Crystal size (mm)	$0.26 \times 0.25 \times 0.03$	$0.09 \times 0.05 \times 0.03$
μ (mm^{-1})	11.371	9.956
θ_{max} (°)	30.0	25.4
Temperature (K)	200	200
N_{cell}	91027	28326
$N_{collected}$	94573	32386
N_{unique}	13252	9413
N_{obs}	8453	5561
Absorption corr	Integration	Integration
T_{min}, T_{max}	0.075, 0.71	0.44, 0.79
Number of parameters	545	383
R [a]	0.036 ($I>2\sigma(I)$)	0.058 ($I>3\sigma(I)$)
R_w [b]	0.043 ($I>2\sigma(I)$)	0.078 ($I>3\sigma(I)$)
Weighting scheme, w	$[\sigma^2(F_o) + 0.0001\lvert F_o\rvert^2]^{-1}$	$[\sigma^2(F_o) + 0.0004\lvert F_o\rvert^2]^{-1}$
$(\Delta/\rho)_{min}$ (e Å^{-3})	−2.06	−3.17
$(\Delta/\rho)_{max}$ (e Å^{-3})	3.44	3.31

[a] $R = \Sigma\lvert\lvert F_o\rvert - \lvert F_c\rvert\rvert / \Sigma\lvert F_o\rvert$.
[b] $R_w = [(\Sigma w(\lvert F_o\rvert - \lvert F_c\rvert)^2 / \Sigma w F_o^2)]^{1/2}$.

The two reversible one-electron oxidation processes in **2** have been probed by UV–vis-NIR spectroelectrochemistry, representative traces from which are shown in Figs. 3 and 4. Electronic absorption spectra acquired while maintaining the potential at 0.50 V (Fig. 3) reveal the isosbestic disappearance of bands centred at 21 000, 25 000 and 32 000 cm^{-1}, and simultaneous appearance of a low intensity low-energy band at 14 500 cm^{-1}, while maintaining the overall appearance of the electronic spectrum (strong bands at high energy tailing to weak bands at lower energy, and spectral transparence

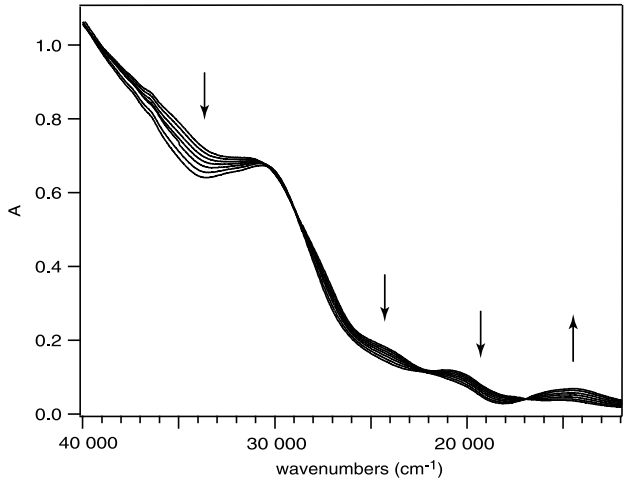

Fig. 3. UV–vis-NIR spectra of $W_2Ir_2(\mu\text{-dppe})(CO)_8(\eta^5\text{-}C_5H_4Me)_2$ (**2**) [CH_2Cl_2, 0.25 M $(NBu^n_4)PF_6$] during exhaustive oxidation ($0 \rightarrow 1+$) at E_{appl}0.50 V at 233 K.

at energies below 10 000 cm^{-1}). Increasing the potential to 0.85 V (Fig. 4) results in isosbestic disappearance of bands centred at 22 000 and 30 500 cm^{-1} and simultaneous appearance of a similar intensity band at 17 500 cm^{-1}; the low-intensity low-energy band at 14 500 cm^{-1} maintains its features on proceeding from $\mathbf{2}^+$ to $\mathbf{2}^{2+}$.

We have previously carried out a detailed UV–vis-NIR and IR spectroelectrochemical study of the reversible conversion of $W_2Ir_2(CO)_{10}(\eta^5\text{-}C_5H_4Me)_2$ (**1**) to $[W_2Ir_2(CO)_{10}(\eta^5\text{-}C_5H_4Me)_2]^+$ ($\mathbf{1}^+$); UV–vis-NIR traces were similar to the present conversion of **2** to $\mathbf{2}^+$, IR traces revealed that the neutral species exists in solution as an isomer mixture including an isomer with bridging carbonyls whereas the oxidized form has an all-terminal carbonyl disposition, and complementary approximate DFT calculations are consistent with retention of the tetrahedral core geometry on oxidation and assignment of the low-energy transition in the oxidized form as $\sigma(W\text{–}W) \rightarrow \sigma^*(W\text{–}W)$ in nature [1]. It is probable in the present case that the $\mathbf{2} \rightarrow \mathbf{2}^+$ and $\mathbf{2}^+ \rightarrow \mathbf{2}^{2+}$ progressions proceed with retention of tetrahedral geometry, that the low-energy bands for $\mathbf{2}^+$ and $\mathbf{2}^{2+}$ are possibly $\sigma(W\text{–}W) \rightarrow \sigma^*(W\text{–}W)$ in composition, and that the stabilization of the second oxidation processes c.f. the precursor cluster results from incorporation of the elec-

Table 4
Cyclic voltammetric data for **1**–**3**, **6**

Cluster	Oxidations, $E_{1/2}$ [$E_pf - E_pr$ mV]			Reduction (E_p)	Ref.
$W_2Ir_2(CO)_{10}(\eta^5\text{-}C_5H_4Me)_2$ (**1**)	–	1.00 [a]	0.70 [70] (1e)	−1.50 (2e) [a]	[1]
$W_2Ir_2(CO)_9(PMe_3)(\eta^5\text{-}C_5H_4Me)_2$ (**6**)	–	0.74 [70] (1e)	0.51 [60] (1e)	−1.68 (2e) [a]	[1]
$W_2Ir_2(\mu\text{-dppe})(CO)_8(\eta^5\text{-}C_5H_4Me)_2$ (**2**)	–	0.61 [70] (1e)	0.35 [120] (1e)	−1.92 (2e) [a]	This work
$W_2Ir_2(\mu\text{-dppf})(CO)_8(\eta^5\text{-}C_5H_4Me)_2$ (**3**)	1.55 [a]	0.70 [70] (1e)	0.35 [80] (1e)	−1.65 (2e) [a]	This work

[a] Irreversible process, E_p.

tron-donating diphosphine, providing a further example of the tuning of cluster electronic properties by co-ligand modification.

3. Experimental

Reactions were performed under an atmosphere of nitrogen using standard Schlenk techniques [16]. All cluster complexes proved to be indefinitely stable in air as solids and for at least short periods of time in solution, and thus no precautions were taken to exclude air in their manipulation. The CH_2Cl_2 reaction solvent (AR grade) was dried over CaH_2 and distilled under nitrogen. Petroleum spirit refers to a petroleum fraction of boiling range 60–80 °C. The $W_2Ir_2(CO)_{10}(\eta^5\text{-}C_5H_4Me)_2$ was prepared using a literature procedure [17]. 1,2-Bis(diphenylphosphino)ethane (dppe) and 1,1′-bis(diphenylphosphino)ferrocene (dppf) were purchased commercially from Aldrich and used as received. The products were purified by thin-layer chromatography (TLC) on 20×20 cm glass plates coated with Merck GF_{254} silica gel (0.5 mm). Analytical TLC, used for monitoring the extent of reaction, was carried out on aluminium sheets coated with 0.25 mm silica gel.

Infrared spectra were recorded on a Perkin–Elmer System 2000 FTIR with CaF_2 solution cells; spectral frequencies are recorded in cm^{-1}. All analytical spectra were recorded as solutions in cyclohexane (AR grade). ^{1}H-NMR and ^{31}P-NMR spectra were recorded in $CDCl_3$ (Cambridge Isotope Laboratories) using a Varian Gemini-300 spectrometer (^{1}H, 300 MHz; ^{31}P, 121 MHz) and are referenced to residual $CHCl_3$ (7.24 ppm) or external H_3PO_4 (0.0 ppm), respectively. Secondary ion mass spectra (SIMS) were recorded using a VG ZAB 2SEQ instrument (30 kV Cs^+ ions, current 1 mA, accelerating potential 8 kV, 3-nitrobenzyl alcohol matrix) at the Research School of Chemistry, Australian National University. All SIMS were calculated with m/z based on ^{183}W and ^{192}Ir assignments, and are reported in the form: m/z (assignment, relative intensity). Elemental microanalyses were carried out by the Microanalysis Service Unit in the Research School of Chemistry, Australian National University.

3.1. Reaction of $W_2Ir_2(CO)_{10}(\eta^5\text{-}C_5H_4Me)_2$ with dppe

A red–brown solution of $W_2Ir_2(CO)_{10}(\eta^5\text{-}C_5H_4Me)_2$ (65.8 mg, 0.0553 mmol) and dppe (22.1 mg, 0.0555 mmol) in CH_2Cl_2 (20 ml) was stirred at room temperature (r.t.) for 18 h. The solution was taken to dryness in vacuo, and the residue was extracted into a small volume (ca. 2 ml) of CH_2Cl_2 and applied to preparative TLC plates. Elution with CH_2Cl_2–petroleum spirit (4/1) gave two bands:

The contents of the first and major band ($R_f = 0.55$) were extracted with CH_2Cl_2 and recrystallized from CH_2Cl_2–methanol at 3 °C to afford red–brown crystals of $W_2Ir_2(\mu\text{-dppe})(CO)_8(\eta^5\text{-}C_5H_4Me)_2$ (**2**) (43.7 mg, 0.0285 mmol, 52%). A crystal grown by this method was selected for a single-crystal X-ray structural study. IR (CH_2Cl_2): ν(CO) 1994vs, 1970vs, 1937m, 1892s, 1814m, 1780s, 1744m, 1711s cm^{-1}. ^{1}H-NMR ($CDCl_3$): δ 8.00–7.15 (m, 20H, Ph), 4.96–3.21 (7 × m, 12H,

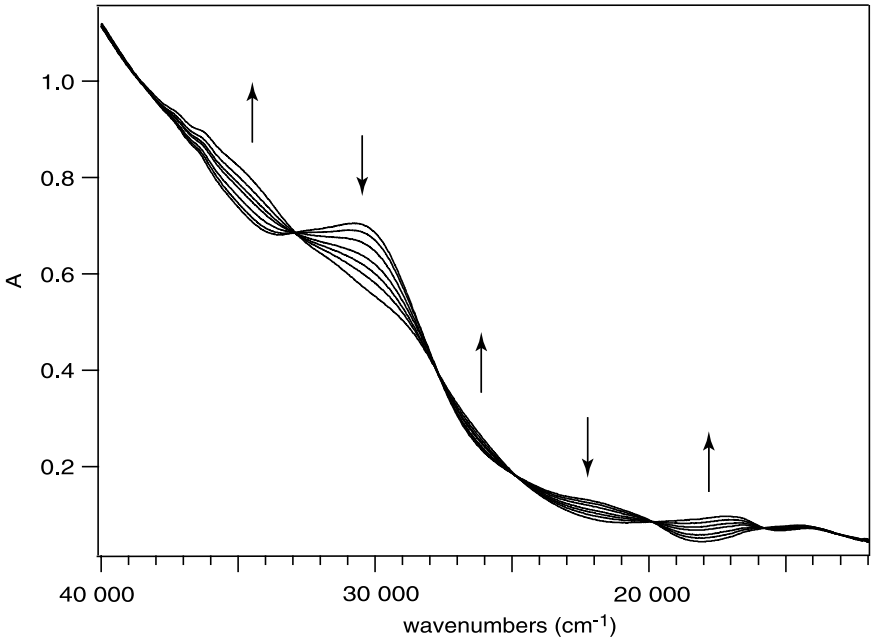

Fig. 4. UV–vis-NIR spectra of $W_2Ir_2(\mu\text{-dppe})(CO)_8(\eta^5\text{-}C_5H_4Me)_2$ (**2**) [CH_2Cl_2, 0.25 M $(NBu^n_4)PF_6$] during exhaustive oxidation (1+ → 2+) at E_{appl}0.85 V at 233 K.

C_5H_4Me, PCH_2), 2.10, 2.04 (2 × s, 6H, C_5H_4Me), 1.56 (s, 2H, H_2O). ^{31}P-NMR ($CDCl_3$): 3.2 (br s), −0.3 (br s), −17.4 (br s), −25.3 (br s). MS (SI): 1530 ($[M]^+$, 11), 1502 ($[M-CO]^+$, 3), 1474 ($[M-2CO]^+$, 11), 1446 ($[M-3CO]^+$, 60), 1418 ($[M-4CO]^+$, 8), 1389 ($[M-5CO-H]^+$, 48), 1361 ($[M-6CO-H]^+$, 26), 1332 ($[M-7CO-2H]^+$, 32), 1304 ($[M-8CO-2H]^+$, 14). Anal. Calc. for $C_{46}H_{38}Ir_2O_8P_2W_2 \cdot H_2O$ (1532.85 + 18.02): C, 35.63; H, 2.60. Found: C, 35.18; H, 2.39%.

3.2. Reaction of $W_2Ir_2(CO)_{10}(\eta^5\text{-}C_5H_4Me)_2$ with dppf

A red–brown solution of $W_2Ir_2(CO)_{10}(\eta^5\text{-}C_5H_4Me)_2$ (91.6 mg, 0.0769 mmol) and dppf (42.5 mg, 0.0767 mmol) in CH_2Cl_2 (15 ml) was stirred at r.t. for 16 h. The brown solution was taken to dryness in vacuo, and the residue was extracted into a small volume (ca. 2 ml) of CH_2Cl_2 and applied to preparative TLC plates. Elution with CH_2Cl_2–petroleum spirit (2/1) gave two bands:

The contents of the first and major band ($R_f = 0.64$) were extracted with CH_2Cl_2 and recrystallized from CH_2Cl_2–methanol at 3 °C to afford dark brown crystals of $W_2Ir_2(\mu\text{-dppf})(CO)_8(\eta^5\text{-}C_5H_4Me)_2$ (**3**) (85.4 mg, 0.0506 mmol, 66%). A crystal grown by this method was selected for a single-crystal X-ray structural study. IR (CH_2Cl_2): ν(CO) 2061s, 2025vs, 2001vs, 1991sh, 1964m, 1940m, 1921m, 1885w, 1817w, 1742w (br) cm^{-1}. ^{1}H-NMR ($CDCl_3$): δ 7.70–7.25 (m, 20H, Ph), 5.23–3.89 (m, 16H, C_5H_4Me, C_5H_4P), 2.12 (s, 6H, C_5H_4Me). ^{31}P-NMR ($CDCl_3$): −19.9 (br s, 2P). MS (SI): 1686 ($[M]^+$, 63), 1630 ($[M-2CO]^+$, 9), 1602 ($[M-3CO]^+$, 5), 1574 ($[M-4CO]^+$, 2), 1546 ($[M-5CO]^+$, 77), 1518 ($[M-6CO]^+$, 20), 1490 ($[M-7CO]^+$, 18). Anal. Calc. for $C_{54}H_{42}FeIr_2O_8P_2W_2 \cdot CHCl_3$ (1688.82 + 119.38): C, 36.54; H, 2.40. Found: C, 36.51; H, 2.74%.

3.3. Electrochemical studies

The cyclic voltammograms were recorded using a MacLab 400 interface and MacLab potentiostat from ADInstruments. The supporting electrolyte was 0.25 M $(NBu^n_4)PF_6$ in distilled, deoxygenated CH_2Cl_2. Solutions containing ca 2×10^{-3} mol l^{-1} complex were maintained under Ar. Measurements were carried out using a platinum disc working-, platinum auxiliary- and Ag | AgCl reference electrodes, using the ferrocene | ferrocenium redox couple as an internal reference (0.56 V). The controlled potential coulometry experiments were carried out using a PAR 273A potentiostat connected to platinum gauze working and auxiliary electrodes, and Ag | AgCl reference electrode in a two compartment (5 ml) electrolytic cell. The UV–Vis spectroelectrochemical spectra were recorded on a Cary 5E spectrophotometer over the range 10 000–40 000 cm^{-1} (1000–250 nm). Solution spectra of the oxidized species at 233 K were obtained by electrogeneration (Thompson 401E potentiostat) at a Pt gauze working electrode within a cryostatted optically transparent thin-layer electrochemical (OTTLE) cell, path-length 0.5 mm, mounted within the spectrophotometer [18].

3.4. X-ray crystallographic studies

The crystal and refinement data for compounds **2** and **3** are summarized in Table 3. Crystals suitable for X-ray structural analyses were grown by liquid diffusion techniques from CH_2Cl_2–MeOH at 276 K. A small, inferior specimen of **3** was used in the absence of anything better; the crystals were suspected of solvent loss and were handled promptly and mounted under a coating of oil. For each study, a single crystal was mounted on a fine glass capillary, and data were collected at 200 K on a Nonius KappaCCD diffractometer using graphite-monochromated Mo–K_α ($\lambda = 0.71069$ Å). The unit cell parameters were obtained by least-squares refinement [19] of N_{cell} reflections with $2.9 \leq \theta \leq 30.0°$ (**2**), $2.9 \leq \theta \leq 25.0°$ (**3**). The reduced data [19] were corrected for absorption using numerical methods [20] implemented from within maXus [21]; equivalent reflections were merged. The structures were solved by heavy-atom Patterson methods [22] and expanded using Fourier techniques [23] within the software package teXsan [24]. All non-hydrogen atoms of **2** were refined anisotropically. In view of the poor quality data for **3**, anisotropic displacement parameter refinement was undertaken for Ir, W, Fe, Cl, P and O only; the C atoms were refined isotropically. Hydrogen atoms in both structures were included in idealized positions which were frequently recalculated, but were not refined. The final cycle of full-matrix least-squares refinement was based on N_{obs} reflections and converged to R and R_w.

4. Supplementary material

Crystallographic data for the structural analyses have been deposited with the Cambridge Crystallographic Data Centre, CCDC nos. 173155 (**2**) and 173156 (**3**). Copies of this information may be obtained, free of charge, from The Director, CCDC, 12 Union Road, Cambridge CB2 1E2, UK (Fax: +44-1223-336033; e-mail: deposit@ccd.cam.ac.uk or www: http://www.ccdc.cam.ac.uk).

Acknowledgements

We thank the Australian Research Council (ARC) for financial support in the form of a Large Grant and the funds to purchase the diffractometer, and Johnson-

Matthey Technology Centre for the generous loan of iridium salts. M.G.H. holds an ARC Australian Senior Research Fellowship, N.T.L. was an Australian Postgraduate Awardee, and J.P.B. thanks the Australian–American Fulbright Commission for a Senior Scholar Award.

References

[1] N.T. Lucas, J.P. Blitz, S. Petrie, R. Stranger, M.G. Humphrey, G.A. Heath, V. Otieno-Alego, submitted for publication.
[2] R.D. Adams, in: G. Wilkinson, F.G.A. Stone, E.W. Abel (Eds.), Comprehensive Organometallic Chemistry II, vol. 10, Pergamon, Oxford, 1995.
[3] S.M. Waterman, N.T. Lucas, M.G. Humphrey, Adv. Organomet. Chem. 46 (2000) 47.
[4] J. Lee, M.G. Humphrey, D.C.R. Hockless, B.W. Skelton, A.H. White, Organometallics 12 (1993) 3468.
[5] S.M. Waterman, M.G. Humphrey, V.-A. Tolhurst, B.W. Skelton, A.H. White, D.C.R. Hockless, Organometallics 15 (1996) 934.
[6] N.T. Lucas, I.R. Whittall, M.G. Humphrey, D.C.R. Hockless, M.P.S. Perera, M.L. Williams, J. Organomet. Chem. 540 (1997) 147.
[7] N.T. Lucas, M.G. Humphrey, P.C. Healy, M.L. Williams, J. Organomet. Chem. 545–546 (1997) 519.
[8] S.M. Waterman, M.G. Humphrey, D.C.R. Hockless, J. Organomet. Chem. 555 (1998) 25.
[9] S.M. Waterman, M.G. Humphrey, D.C.R. Hockless, J. Organomet. Chem. 565 (1998) 81.
[10] S.M. Waterman, M.G. Humphrey, Organometallics 18 (1999) 3116.
[11] S.M. Waterman, M.G. Humphrey, J. Lee, G.E. Ball, D.C.R. Hockless, Organometallics 18 (1999) 2440.
[12] S.M. Waterman, M.G. Humphrey, D.C.R. Hockless, J. Organomet. Chem. 582 (1999) 310.
[13] S.M. Waterman, M.G. Humphrey, J. Lee, J. Organomet. Chem. 589 (1999) 226.
[14] R.J. Klingler, W.M. Butler, M.D. Curtis, J. Am. Chem. Soc. 100 (1978) 5034.
[15] M.D. Curtis, K.R. Han, W.M. Butler, Inorg. Chem. 19 (1980) 2096.
[16] D.F. Shriver, M.A. Drezdzon, The Manipulation of Air-Sensitive Compounds, Wiley, New York, 1986.
[17] N.T. Lucas, E.G.A. Notaras, M.G. Humphrey, Acta Crystallogr. E57 (2001) m132.
[18] C.M. Duff, G.A. Heath, Inorg. Chem. 30 (1991) 2528.
[19] Z. Otwinowski, W. Minor (Eds.), Methods in Enzymology, Academic Press, New York, 1997, p. 307.
[20] P. Coppens (Ed.), Crystallographic Computing, Munksgaard, Copenhagen, 1970, p. 255.
[21] S. Mackay, C.J. Gilmore, C. Edwards, N. Stewart, K. Shankland, maXus: Computer Program for the Solution and Refinement of Crystal Structures, Nonius, The Netherlands; MacScience, Japan and The University of Glasgow, UK, 1999.
[22] P.T. Beurskens, G. Admiraal, G. Beurskens, W.P. Bosman, S. Garcia-Granda, R.O. Gould, J.M.M. Smits, C. Smykalla, PATTY: The DIRDIF program system. Technical Report of the Crystallography Laboratory, University of Nijmegen, Nijmegen, The Netherlands, 1992.
[23] P.T. Beurskens, G. Admiraal, G. Beurskens, W.P. Bosman, R. de Gelder, R. Israel, J.M.M. Smits, The DIRDIF-94 Program System. Technical Report of the Crystallography Laboratory, University of Nijmegen, Nijmegen, The Netherlands, 1994
[24] teXsan: Single-Crystal Structure Analysis Software, Version 1.8, Molecular Structure Corporation, The Woodlands, TX 77381, 1997.